ChemPubSoc Europe

DOI: 10.1002/cphc.201500534

CHEMPHYSCHEM Articles

# Mechanostability of the Single-Electron-Transfer Complexes of *Anabaena* Ferredoxin–NADP$^+$ Reductase**

Carlos Marcuello,[a] Rocío de Miguel,[a] Marta Martínez-Júlvez,[b] Carlos Gómez-Moreno,[a, b] and Anabel Lostao*[a, c]

The complexes formed between the flavoenzyme ferredoxin–NADP$^+$ reductase (FNR; NADP$^+$ = nicotinamide adenine dinucleotide phosphate) and its redox protein partners, ferredoxin (Fd) and flavodoxin (Fld), have been analysed by using dynamic force spectroscopy through AFM. A strategy is developed to immobilise proteins on a substrate and AFM tip to optimise the recognition ability. The differences in the recognition efficiency regarding a random attachment procedure, together with nanomechanical results, show two binding models for these systems. The interaction of the reductase with the natural electron donor, Fd, is threefold stronger and its lifetime is longer and more specific than that with the substitute under iron-deficient conditions, Fld. The higher bond probability and two possible dissociation pathways in Fld binding to FNR are probably due to the nature of this complex, which is closer to a dynamic ensemble model. This is in contrast with the one-step dissociation kinetics that has been observed and a specific interaction described for the FNR:Fd complex.

## 1. Introduction

The ability of biomolecules to distinguish and bind specifically to other molecules is referred to as biomolecular recognition and plays a crucial role in various biological processes, such as immunological responses, signalling, molecular assembly, gene expression or cellular adhesion, and remains a central theme in molecular biology. Experimental evidence suggests that ligands select the most favoured receptor conformation. Following binding by a primary conformational selection event, optimisation of side chain and backbone interactions is likely to proceed by an induced fit mechanism. Conformational selection has been observed for protein–ligand, protein–protein, protein–DNA, protein–RNA and RNA–ligand interactions.[1] Analyses of the equilibrium constant and the association and dissociation rate constants have been used to characterise the physicochemical properties of ligand–receptor interactions, although these values are generally coarse-grained data. Acquisition of more detailed physicochemical information related to ligand–receptor interaction forces is required for clarifying the molecular basis of the biochemical interactions as well as the thermodynamic and kinetic parameters. For this task, direct intermolecular force measurement techniques, including AFM,[2,3] micropipette suction,[4] optical tweezers,[5] surface force apparatus[6] and magnetic torsion devices,[7] have been developed and applied for the characterisation of the dynamic response of individual ligand–receptor complexes to external mechanical forces. In recent years, dynamic force spectroscopy (DFS) based on the Bell–Evans (BE) theoretical framework has become a powerful analytical strategy for exploring the energy landscape of ligand–receptor unbinding.[4,8] Nowadays, AFM may provide data on the topology, adhesion, elasticity, dynamics and other properties of biomolecular samples in buffer and is the most currently used approach for DFS studies.[9] DFS provides mechanostability information about the complex formed by protein immobilised on the sample surface and its partner linked onto the cantilever AFM tip by measuring the unbinding force of the complex at different loading rates ($R$).[4] The functionalised tip is moved directly towards the sample until they are in contact, and then retracted again; the interaction between tip and sample is measured by using a force–distance (Fz) curve, Fz scan or Fz curve. This may then be repeated to give full statistical information with respect to the interaction. Non-destructive immobilisation methods are therefore required.[10] For the first cases studied, simplified models were limited to single bonds,[2] but multiple interactions (i.e. van der Waals, hydrogen bonding, ionic and hydrophobic) are involved during the formation–rupture of biocomplex bonds within the binding site, which determine the characteristics of specific binding.

The systems studied herein consist of the complex formed by the flavoenzyme ferredoxin–NADP$^+$ reductase (FNR; NADP$^+$ = nicotinamide adenine dinucleotide phosphate), which contains a flavin adenine dinucleotide (FAD) group and the binding partners ferredoxin (Fd), with a [2Fe–2S] cluster, and flavodoxin (Fld), with a flavin mononucleotide (FMN)

[a] Dr. C. Marcuello, Dr. R. de Miguel, Prof. Dr. C. Gómez-Moreno, Dr. A. Lostao
Laboratorio de Microscopías Avanzadas
Instituto de Nanociencia de Aragón, Universidad de Zaragoza
C/Mariano Esquillor, s/n. Ed. I+D+i, 50018 Zaragoza (Spain)
E-mail: aglostao@unizar.es

[b] Dr. M. Martínez-Júlvez, Prof. Dr. C. Gómez-Moreno
Departamento de Bioquímica y Biología Molecular y Celular
Universidad de Zaragoza, C/Pedro Cerbuna, 12
Facultad de Ciencias, 50009 Zaragoza (Spain)

[c] Dr. A. Lostao
Fundación ARAID, C/María de Luna, 11. Ed. CEEI Aragón
50018 Zaragoza (Spain)

[**] NADP$^+$ = Nicotinamide Adenine Dinucleotide Phosphate

group, from the cyanobacterium *Anabaena* PCC 7119.[11] Fld is an electron-transport protein synthesised under iron deficiency, when the synthesis of Fd is hampered.[12] Two Fd or Fld molecules interact sequentially with FNR for the step-wise transfer of two electrons. Finally, reduced FAD from FNR is used to convert $NADP^+$ into NADPH. Both the enzyme and redox partner form a transient complex to transfer electrons in the photosynthetic electron-transfer (ET) chain. This redox system is particularly interesting because two proteins of different nature (Fd and Fld) interact at the same site of FNR.[13] The results obtained by our group, as well as others, have revealed that this system can be considered as a paradigm for investigating the parameters that determine the complex formation event as well as the ET process involved in the reaction.[11,14,15] However, some aspects of the association mechanism of these redox complexes still remain unclear. Flavoenzymes are oxidoreductases that catalyse a large variety of different types of reactions.[16] These enzymes have been extensively studied for their structural and mechanistic properties. They have a central role in aerobic metabolism through their ability to catalyse both one- and two-ET reactions. Their exploitable functions, such as recognition capability, catalysis and ET, may be combined to fabricate hybrid nanodevices.[17,18]

Herein, we report a comparative analysis on the nanomechanical dissociation parameters from complexes formed from FNR with Fd and Fld by using AFM in the DFS mode. The measurement of rupture forces is often obscured by the lack of molecular mobility, nonspecific bindings or an incorrect orientation of one molecule over another. Although early problems have been solved by using flexible linkers,[10] measurements are still of poor quality due to a very low percentage of rupture events generated during experiments, which is caused by a low yield in biorecognition. Typically, the immobilisation of molecules on AFM tips and samples is performed randomly. This leads many of the immobilised protein molecules being unable to interact with their partners because their interacting surfaces have been used to anchor them to the support, which could be problematic for recognition imaging and very negative in DFS, for which the incorrect orientation of a molecule in a sample over one at the tip results in binding only occurring in a small percentage of approaches. Herein, we introduce the factor of protein orientation to measure intermolecular forces in both protein complexes. The method consists of labelling proteins with a suitable cross-linker once formed the recognition complex, subsequent separation of the marked proteins, and their immobilisation by exposing the interaction surface of one molecule towards the other. This method not only achieves a large increase in successful rupture events, but comparative analysis of Fz efficiency by using oriented and non-oriented molecules allows us to obtain information on the specificity for both complexes.

The results in mechanical stability, lifetime, dissociation kinetic pathway and binding probability data indicate different binding models for the two protein ligands at the same interaction surface. This could suggest that, in iron deficiency, cyanobacteria accelerate the expression of a protein that performs the same function as Fd, which is able to bind to the same site of the enzyme, but in a non-specific and promiscuous manner, less strongly and durably, and transferring electrons less efficiently to preserve the photosynthetic function under unfavourable physiological conditions. This analysis, including the protein labelling procedure, could be applied to other protein–protein systems, particularly redox or transient ET complexes.[19]

## 2. Results

### 2.1. Protein Functionalisation Strategies

The study of the interaction of two proteins by AFM requires that both molecules are strongly attached: one on the AFM substrate and the other to the cantilever tip. The functionalisation strategy designed herein allows the immobilisation of proteins in a random or oriented way. To analyse the effect that the exposition of the active interacting site in FNR could have on the formation of bonds between the two proteins, a series of DFS measurements were performed with different FNR samples presenting free or pyridyldithiopropionamide (PDP)-occupied sites (tag from the PDP part of the cross-linker used; see the section on Protein Labelling in the Experimental Section) to Fd or Fld. Accordingly, FNR samples have been prepared by previous addition of Fd or Fld to form a complex with FNR prior to incubation with PDP. Therefore, this enzyme pool, named $FNR_c$, has a PDP-free binding site. The other sample, named $FNR_r$, has been modified with PDP without any protection of the interacting site, so that it can be immobilised on the mica sheet in any random position. The mixture of FNR and Fd, after PDP labelling, was passed through a size-exclusion chromatography column that yielded $FNR_c$ and $Fd_c$ (from the [FNR:Fd]–PDP complex) in separate fractions; the same quality was obtained by using desalting chromatography to collect $FNR_r$.[20,21] On the other hand, anionic exchange chromatography allowed us to separate $FNR_c$ and $Fld_c$ (from the [FNR:Fld]–PDP complex; results not shown). The immobilisation strategy designed to orient FNR on mica towards Fd was evaluated previously.[20] Homogeneous layers of FNR on the substrates were generated, as observed by AFM imaging. Steady-state enzymatic assays of immobilised FNRs gave data to indicate that the functionality of the samples was not affected by the tagging, separation and immobilising steps. Furthermore, the $FNR_c$ samples showed higher cytochrome *c* reductase activity than those estimated for the $FNR_r$ samples; this was nine times greater, on average, for the tagged enzyme from the complex with Fd.[20] These results are consistent with the efficient targeting method designed, in which most of the enzyme molecules have the correct orientation of their interaction surfaces towards the solution. Tagged Fd and Fld were used to functionalise the AFM probes.

### 2.2. Influence of the Orientation Methodology and Applied Force in Bond Formation and Dissociation

We analysed how the procedures described to attach the proteins to the substrate and probe affected the generation of

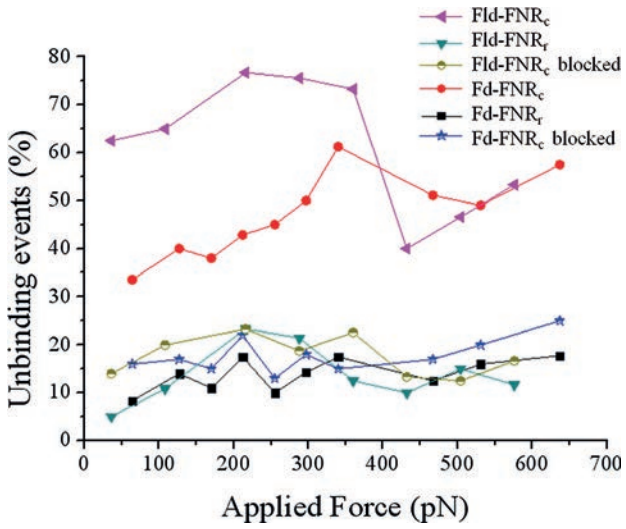


**Figure 1.** Ratio of successful approaches for the dissociation of the complexes in DFS experiments, depending on the loaded force. Higher applied forces were not used to prevent deformation in the protein layers.

rupture events for complexes between FNR and Fd or Fld over a large range of applied forces. Figure 1 shows the percentage of binding events produced upon approaching both couples of proteins at different loading forces. The most relevant data shown refer to a high increase in the percentage for rupture events in approaches when $FNR_c$ samples are used. The results obtained for standard random labelling and attachment are clearly lower and range from 5 to 23%. These data are similar to those found in the literature for these kinds of experiments based on random procedures. These results indicate that an optimum orientation lead to a high efficiency in the formation and subsequent rupture of bonds between both site-oriented pairs. Control experiments with an excess of Fld to block the FNR binding sites gave an important decrease in rupture events, probing the specificity of the measurements. In our case, we have used Fld covering the FNR samples for both Fd- and Fld-functionalised tips. Fld is an easier protein to produce and previous data clearly show that Fd and Fld share the same interaction area on FNR.[13]

The efficiency in the approaches with oriented molecules was so high that, even when these samples were blocked with free ligand, the yield was still slightly higher than that for randomly immobilised enzyme samples (Figure 1). Nevertheless, there are some differences between both types of complexes. The efficiency reached in the approaches with Fld-tagged tips was in the range of 40–77%, whereas that with Fd-tagged tips reached 34–61% (Figure 1). On the other hand, the increase for the randomly functionalised samples oscillated between 3–13 and only 2–4 times for Fld and Fd approaches, respectively. The highest effectiveness for the Fld complex occurred at around 216 pN of applied force, whereas the maximum percentage of specific rupture events with Fd was found at approximately 340 pN loaded force.

### 2.3. Mechanical Stability of the FNR Complexes

Fz curves provide reliable information about the interaction process and present a large variability due to its intrinsic stochastic nature (random or non-deterministic process). This requires the measurement of thousands of curves with different $R$ and to apply a statistical analysis to the curves by assuming that $R$ remains constant from one measurement to the next. It is also necessary to discard all those signals that do not reflect specific interactions and also those ambiguous ones that are considered to be "false events". Each asymmetrical force histogram can be grouped under two or three different peaks fitted to Gaussian curves. The rupture events taking place at the lowest force values could be those interactions that account for the participation of a single couple of proteins. Those rupture events observed at intermediate force values would be the ones in which two protein couples bind the sample and tip in the AFM apparatus. Thus, the force required to break the bond is approximately double that required for a single event. The third peak shows the events in which three proteins and their couples interact simultaneously. In this case, the force required is around three times that for the single event. The analysis indicates two clear trends for both types of FNR complexes (Figure 2). Increasing $R$, first, always results in higher unbinding forces and, second, the appearance of multiple peaks decreases. Figure 2 shows three selected histograms obtained at different $R$ values for the FNR:Fd (Figure 2a–c) and FNR:Fld (Figure 2d–f) complexes. These histograms are representative of the whole series. It can be observed that the bond probability increases at low $R$ for both complexes, which exhibit a tendency for multi-peaks to disappear at higher velocities. These results suggest that the slower approach and withdrawal of the tip to the sample favours the formation of bonds because the ligands remain close to the receptors at the sample for longer, which increases the encounter probability; hence, the number of multiple events increases. The multiple peaks effect was high in this work, in comparison with other studies,[4] at any velocity thanks to the use of oriented molecules on the tip and sample to increase the probability of an encounter.

The quality of the analysis may be also evaluated by blocking experiments. The fitting of the resulting histograms have very similar maxima data to those from non-blocked samples at the same velocity, but decreasing the absolute rupture events frequency, as can be seen in Figure 3, which shows the relative force frequencies for the FNR:Fd complex at $R = 10\ nN\,s^{-1}$. As the effectiveness decreases, a relative increase in the single events compared with multiple events or simultaneous rupture of several molecular complexes is produced. The results obtained from the blocking experiments and multiple peaks in the histograms are clearly indicative of the specificity of the measurements.

Regarding the force data, the intermolecular forces found for the complex with Fd are higher than those estimated for the complex with Fld for the wide velocity range analysed (Figure 4). At $R = 10\ nN\,s^{-1}$, $(57 \pm 16)$ and $(21 \pm 8)$ pN were obtained as the most probable unbinding forces for a single FNR complex with Fd and Fld, respectively (Table 1).

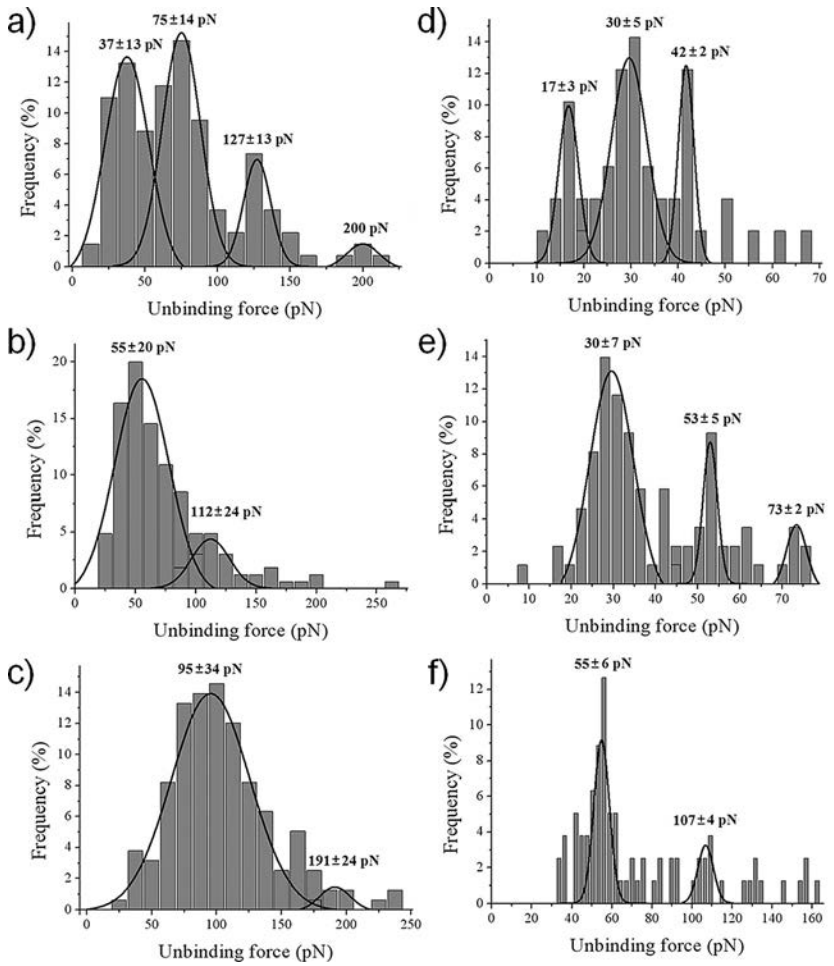


**Figure 2.** Representative force histogram distributions for the FNR:Fd (a–c) and FNR:Fld (d–f) complexes operating at $R$ values of 3 (a,d), 20 (b,e) and 78 nN s$^{-1}$ (c,f). The width of the bars varies in each case, depending on an optimum fit. The probability of generating multiple events decreases similarly for both complexes as $R$ increases.

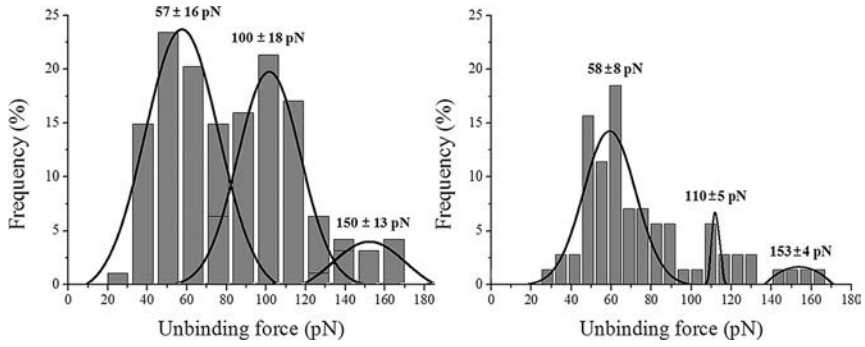


**Figure 3.** Control experiment showing histograms obtained at $R = 10$ nN s$^{-1}$ for the FNR:Fd complex (a) and the corresponding blocked sample with excess of ligand (b). The width of the bars varies in each case, depending on an optimum fit.

### 2.4. Molecular Recognition Imaging

Operation with jumping mode (JM) in repulsive regime minimises unspecific tip–sample interactions. This strategy allows us to obtain adhesion images in which rupture force events correlate with topology height events in the topography homologous maps.[22,23] Figure 5 shows representative images of $FNR_c$ samples scanned with the protein-attached tips; these images allow us to observe directly adhesion features that may be attributed to specific rupture forces of the complexes. Molecular recognition images show multiple and single peak features that follow the same characteristics of DFS data, which also have unbinding values in the same range. It can be also observed that the rupture-force values for FNR:Fd complexes are higher (Figure 5a and b) than those found for FNR:Fld complexes (Figure 5c and d). It is possible to assign the smaller values to rupture of single complexes and subsequently attribute greater values to multiple peaks, which are typically two ruptures. The good correlation between topography and adhesion is favoured by using an enzyme immobilised with the interaction surface facing the ligand at the tip.

### 2.5. Dissociation Kinetics for the FNR Complexes

The energy landscape of bond rupture explored by DFS characterises the force-driven pathway along the pulling direction until the bond ruptures. A classical representation of the energy landscape is made in a one-dimensional plot representing the energy of the system versus the reaction coordinate.[24]

The shape of the energy landscape is thus constituted by the height of energy barriers, characterised by a $k_{off}$ value, and the energy barrier width, called $x_\beta$, between the valley and summit of the mountain. BE plots are obtained when the dependence of the rupture force on $R$ is represented. In the simplest case, in which a single bond between ligand and receptor is measured, the BE plot exhibits a single linear fit, which shows the increase in the most probable rupture forces as a function of a logarithm of $R$. The slope of the fit is equal to $k_\beta T/x_\beta$, in which $k\beta$ is the Boltzmann constant, $T$ is the temperature and $x_\beta$ (in Å) is the distance from the energy minimum to the transition state. When the measured interaction involves multiple bonds, the

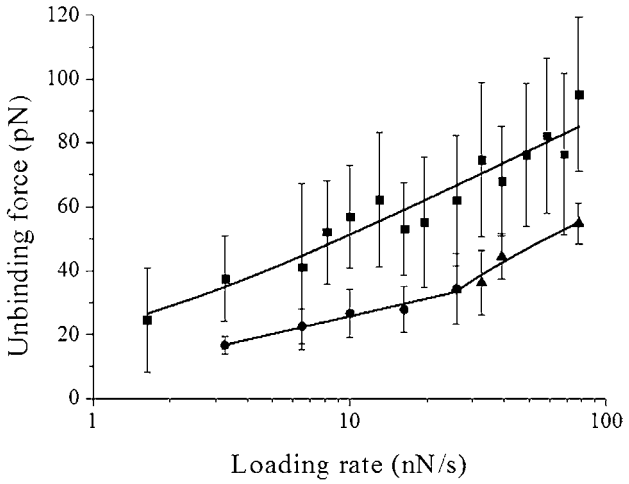


**Figure 4.** Loading-rate dependence of the most probable unbinding forces. The unbinding forces correspond to the rupture of single complexes that result from a Gaussian fit to the histogram distributions. Force statistical errors are given by standard deviation. The solid lines correspond to numerical fits of experimental data to the BE model. The FNR:Fd complex (squares) presents one slope, whereas the FNR:Fld complex (circles and triangles) fits better to two slopes. Best-fitting nanomechanical parameters are shown in Table 1.

**Table 1.** Mechanical parameters for the dissociation of FNR:Fd and FNR:Fld complexes. The values were obtained from fitting of the data shown in Figure 4. Assays were performed in phosphate-buffered saline (PBS)/ethylenediaminetetraacetic acid (EDTA), pH 7.0.

| Complex | Unbinding force [pN][a] | $k_{off}$ [$s^{-1}$] | $\tau$ [s] | $x_\beta$ [nm] |
|---|---|---|---|---|
| FNR:Fd | $57\pm16$ | 21.2 | 0.047 | $0.27\pm0.01$ |
| FNR:Fld (1) | $21\pm8$ | 55.7 | 0.018 | $0.47\pm0.02$ |
| FNR:Fld (2) | | 253.3 | 0.004 | $0.18\pm0.01$ |

[a] Values corresponding to the rupture of a single complex, at $R=10$ nN $s^{-1}$.

BE plot could exhibit several linear fits that correspond to multiple parallel bonds. Multiple bonds may originate from multivalent systems (antibodies) or from multiple ligand–receptor interactions, depending on the density of ligands and receptors. The BE plots allows us to obtain the kinetic dissociation constant, $k_{off}$, which is calculated from the extrapolation of the fitting to force zero. The representation of the most probable unbinding forces as a function of $R$ exhibited one and two distinct linear regimes for the Fd and Fld complexes, respectively (Figure 4). Such behaviour can be traced back to the presence of one and two intermediate states in the dissociation process, according to one or two energy barriers.[25] Although the dispersion of data in the FNR:Fd complex is considerably higher, from the BE plot it is still possible to clearly define a linear fit. Therefore, Fd dissociates from FNR through a single energy barrier between the initial state and the transition state of the highest energy to which the system must be raised before dissociation can occur. However, Fld needs to pass through a pathway of two energy barriers to be dissociated from FNR and two $k_{off}$ values have been extracted by two independent linear fits. This means that an inner energy barrier is crossed first followed by a second outer energy barrier.[26] The outer energy barrier can be observed by applying low $R$, opposite to the inner energy barrier, which appears at high $R$. Furthermore, $k_{off}$ is related to the characteristic lifetime, $\tau_o$, of the complex ($\tau_o = k_{off}^{-1}$).

Table 1 also shows the estimated lifetimes for the single complexes. The expected lifetime for a FNR:Fd complex is almost three times that expected for a FNR:Fld complex. These data provide information on the specificity of the reaction. Specificity refers to the ability of a protein to bind one molecule in preference to another molecule to perform a task. It is thought that higher lifetimes,[27–29] interaction forces, and affinities, characterised by the equilibrium constants, are related to greater specificity in the biorecognition processes. Analyses

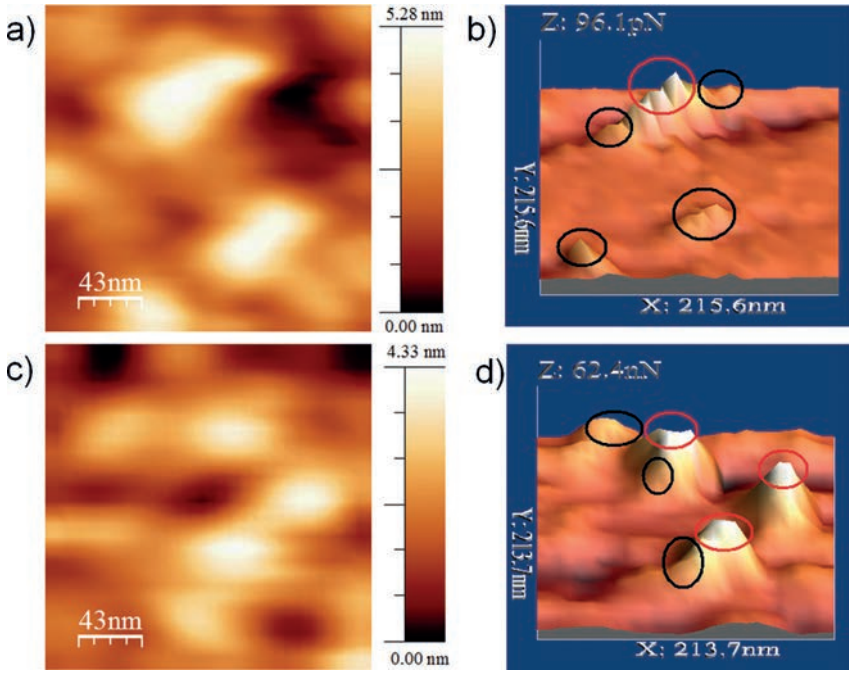


**Figure 5.** Simultaneous topography (a,c) and adhesion maps (b,d) of an $FNR_c$ sample scanned by using Fd- (a,b) and Fld-functionalised (c,d) probes in JM-AFM mode under repulsion conditions. FNR molecules are resolved in the topography maps. The adhesion peaks in the 3D adhesion maps are due to molecular recognition events. Forces due to the simultaneous rupture of two complexes are surrounded by red circles, whereas single events are highlighted by black circles.

give a position of the energy barrier along the reaction coordinate, $x_\beta$, of $(0.27 \pm 0.01)$ nm for FNR:Fd, and $(0.47 \pm 0.02)$ and $(0.18 \pm 0.01)$ nm for FNR:Fld.

## 3. Discussion

Typical force spectroscopy measurements were performed on a flavoenzyme system involved in ET processes. The main aim of these experiments was to gather further information on the mechanical properties of these specific protein–protein complexes and establish a basis for the study of other ET protein complexes. The experiments consisted of the recording of multiple Fz curves by approaching the Fd/Fld functionalised tips to FNR samples. Herein, the introduction of factor orientation in the functionalisation of the molecular partners was used to optimise the general efficiency in the measurements and it also provided certain information on molecular binding. For both complexes, the binding efficiency on approach was significantly higher when FNR was immobilised in an oriented fashion; this led to, on average for the whole *R* range explored, around 61% of successful rupture events. This ratio decreased to around 20% when using randomly immobilised FNR (Figure 1). Orientation not only improves DFS, but also provides direct evidence that the measured force comes from the interaction between the two partner proteins. It can be extracted that this is specific binding produced through the recognition of a specific area in FNR protected by Fd/Fld during the preparation of the $FNR_c$–PDP species. These results also indicate that the efficiency of the binding events obtained for the $FNR_c$–PDP samples drops to a level similar to that of randomly modified samples when the site for the interaction is protected by the partner protein, Fld, in the blocking measurements. A similar increase was observed in the rate of cytochrome *c* reductase activity given by $FNR_c$, with regard to $FNR_r$, not only on the surface, but also in solution,[20] and also in molecular recognition imaging (Figure 5). These results are consistent upon considering that the three approaches require the formation of FNR:Fd or FNR:Fld complexes, and therefore, depend on the accessibility of the ligand to the surface interaction at the receptor. Nevertheless, the increase in binding events was further achieved when Fld was attached to the tip, and reached almost 80% of the approach events, whereas Fd tips did not exceed 61% when using $FNR_c$ samples (Figure 1).

The different results found for both complexes agree with previous kinetic data, which suggests that the interaction between FNR and Fd is highly specific and site-localised with salt bridges between certain key positive residues on FNR and negative residues on Fd,[11,30] which contribute with other non-specific interactions, such as hydrogen bonds or the hydrophobic effect. On the contrary, kinetic and docking studies on variants indicate that Fld can adopt multiple orientations on the FNR surface to be effective in binding and subsequent ET, with no evidence of specific interactions between residues from both proteins on the interaction surface so far.[11,17,18,30,31] On the other hand, the highest effectiveness for Fld complex formation occurs when a force of around 216 pN is applied, relative to 340 pN for Fd. The difference found could be attributed to a greater difficulty in forming a more specific complex, with a more localised binding area with Fd (Figure 1). Despite their differences, Fd and Fld bind to FNR through similar energetics. The main significant gaps are related to polarity and size of the recognition interface: an individual Fd molecule removes 30 water molecules and a single Fld molecule liberates 20 water molecules upon binding to FNR.[15] Fd binds to a larger region in FNR and its residues are more critical in interactions than those of Fld. The high effectiveness in the measurements is attributed to the appearance of forces that are multiples of the first peak, which exhibits the lowest value and indicates single, double and triple events (Figures 2 and 3). The same trends can be observed qualitatively in the molecular recognition images (Figure 5). The occurrence of multiple events requires the contact of the two components of several complexes to be maintained for long enough to allow the interaction forces to be established. This is clearly observed in experiments in which histograms of the unbinding events at different *R* values are presented (Figure 2). In this case, we can observe that the number of multiple events decreases as *R* increases. Furthermore, force histograms demonstrate not only a shift in peak location, but an increase in width as *R* increases, as observed in other systems.[32] It is interesting to note that the unbinding forces obtained in the blocking measurements are almost exactly the same as in the case of freely exposed samples, although the frequency of the multiple events is clearly lower than in the case of the protected protein (Figure 3). Thus, for single events in the dissociation of the FNR:Fd complex at $R = 10\ nN\,s^{-1}$, forces of $(57 \pm 16)$ and $(58 \pm 8)$ pN were obtained, which demonstrated specificity in the measurements (Figure 3). Regarding dissociation, the distance from the energy minimum to the transition state is lower in the case of the Fd complex than that of the Fld one. This could mean that the distances between both protein centres were smaller than those for Fld, which could be related to previous analysis that estimated the distance between the respective redox centres to be 0.41 nm for the FNR:Fd structure and 0.74 nm for the FNR:Fld model.[33] With the observation of the plot in Figure 4, one can see that the unbinding forces in the FNR:Fd complex are higher than those found for the FNR:Fld complex. In particular, the mechanical stability of the Fd complex is almost three times stronger than that exhibited by the complex formed with Fld (at $R = 10\ nN\,s^{-1}$) and its lifetime is also three times longer. Compared with other biomolecular complexes, the intermolecular forces that maintain the FNR systems are low, which is consistent with its nature as transient redox complexes that involve weak interactions.[34] The strength of the FNR:Fd complex is comparable to less stable antigen–antibody complexes, which span a wide range of 30 to 250 pN, such as ferritin–antiferritin, showing a force of 50 pN[35] and lysozyme–antilysozyme variable fragment (Fv) with 55 pN[36] at $R = 10\ nN\,s^{-1}$. With regard to the FNR:Fld complex, its mechanical stability is similar to that found for systems involved in adhesion processes, such as αβ-integrin-GRGDSP peptide (20 pN[37]) and cadherin–cadherin (with 35 pN[38]) at the same *R* value. In the case of the FNR:Fld complex, there are two *R* regimes, or two intermediate states, whereas in the

FNR:Fd complex a single regime is found in the dissociation process (Figure 4). This means that in the first case an inner energy barrier is crossed first followed by a second outer energy barrier.[26] The outer energy barrier can be observed by applying a low *R* value, opposite to the inner energy barrier, which appears at high *R*. This may be attributed to the fact that Fld can associate with FNR in more than one optimum orientation to transfer electrons in the redox reaction.[31] In all these possible orientations, the two flavin cofactors are at a very short distance once the complex is formed, facilitating the reaction between the two redox centres in this way;[11] meanwhile, Fd only supports one specific orientation in FNR binding. The $k_{off}$ values were estimated to be 21.2 $s^{-1}$ for the Fd complex, and 55.7 and 253.3 $s^{-1}$ for the Fld complex; these values are not as high as that of the typical $k_{off}$ expected for ET transient complexes.[19] Sometimes the differences between the $k_{off}$ values obtained by DFS and those derived from bulk techniques, such as surface plasmon resonance (SPR), can be evidenced.[34] Therefore, it is less problematic to compare only $k_{off}$ data estimated by DFS for different complexes. Our data are, however, much higher than the off rates typically estimated by DFS for stable ligand–receptor pairs, such as antigen–antibody pairs in the range of 0.01 $s^{-1}$. On the other hand, it is commonly accepted that ET complexes have high $k_{off}$ (as well as $k_{on}$) values, with typical values of up to $10^3$ $s^{-1}$ (whereas $k_{on}$ is in the range of $10^7$–$10^9$ $M^{-1}$ $s^{-1}$).[19] Such peculiarity renders the FNR complexes different from most complexes usually studied by DFS experiments, which are more stable. This feature was also observed for the azurin-$C_{551}$ ET complex, with a value of 14 $s^{-1}$,[39] which was in the same range as those of the FNR systems.

## 4. Conclusions

It is interesting to note that plastocyanin and cytochrome $c_6$ are two metalloproteins that act as alternative electron carriers between cytochrome $b_6$f and photosystem I, also in *Anabaena,* which choose plastocyanin when copper is available. These proteins have similar sizes and midpoint redox potentials, and several residues similarly conserved in both are critical for the ET reaction with photosystem I, which easily explains their functional homology.[40] However, the system chosen for nanomechanical analysis is paradigmatic for the study of the association/dissociation mechanism of redox complexes because two proteins with different sizes, structures and redox centres (Fd and Fld) bind to the same interaction site of FNR.[13]

Herein, we introduced the factor of protein orientation, which not only allowed us to achieve a large increase in successful rupture events, but also perform a comparative analysis on Fz efficiency by using oriented and non-oriented proteins to obtain data on the specificity of the complexes. The results indicated that the FNR:Fd complex was more specific, mechanically stronger and more durable than that of FNR:Fld; Fd dissociated from FNR through a single barrier and Fld followed two barriers. The probability of establishing binding by Fld was higher than that for Fd. This attested to two different binding models for two protein ligands at the same surface. These data, together with previous biophysical results, could suggest that, when cyanobacteria detected an iron decrease, they would express a protein able to perform the same function as that of Fd. Fld bound to the same site of the enzyme, but through a nonspecific and promiscuous route, which presented a higher binding probability for the enzyme to form a weaker association, and transferred electrons less efficiently to preserve the photosynthetic function under unfavourable physiological conditions. This analysis, including the protein-labelling procedure, could be applied to other protein–protein systems, particularly redox or transients ET complexes.

## Experimental Section

### Protein Labelling and Immobilisation of FNR on Mica

Recombinant FNR, Fld and Fd proteins from *Anabaena* were purified from *Escherichia coli* cultures containing recombinant DNA with the corresponding encoded genes.[12,13] The enzyme was modified with 20 mM sulfosuccinimidyl 6-(3′-[2-pyridyldithio]propionamido)hexanoate (Sulfo-LC-SPDP; Pierce) following two strategies, namely, direct use and after incubation with the protein partner, Fd or Fld, in a 1:2 ratio. In the first strategy, the protein surface was randomly coated with the tag (the resulting species is labelled herein as $FNR_r$–PDP). Alternatively, the FNR molecule surface was coated with the PDP tag, except in the interface area, which was covered by the protein partner, free from the tag (this species is labelled herein as $FNR_c$–PDP). The complex [FNR:Fd]–PDP was treated with 0.5 M NaCl and separated by size-exclusion chromatography with a Superdex 75 column (GE Healthcare) equilibrated in 50 mM Tris/HCl, 250 mM NaCl, pH 8.0, in one step to yield isolated $FNR_c$–PDP and $Fd_c$–PDP.[20,21] $FNR_r$–PDP was purified by using a Sephadex G-25 desalting chromatography (GE Healthcare) performed in 50 mM Tris/HCl, pH 8.0. The production of $FNR_c$ and $Fld_c$ was performed by using a similar procedure of incubation of both proteins prior to the addition of PDP. Then elution of the [FNR:Fld]–PDP complex through anionic exchange chromatography on a Mono Q column (GE Healthcare) in 50 mM Tris/HCl, pH 8.0, with a gradient from 0 to 750 mM NaCl to separate the tagged proteins. The purity of the fractions was checked by sodium dodecyl sulfate polyacrylamide gel electrophoresis (SDS-PAGE) with a gradient of 8–25% in a PhastSystem (GE Healthcare) by using a low-molecular-weight Market kit as a reference (GE Healthcare). The immobilisation of $FNR_r$ and $FNR_c$ (from labelling of both FNR:Fd and FNR:Fld complexes) was developed on muscovite mica (Electron Microscopy Sciences). Freshly cleaved pieces were exposed to vapours of 3-aminopropyl triethoxysilane (APTES; Sigma–Aldrich) and *N*,*N*-diisopropylethylamine (Hünig's base; Sigma–Aldrich) under an argon atmosphere. 20 mM Sulfo-LC-SPDP in PBS/EDTA-azide (Pierce) was added to the aminated mica at room temperature. The exposed PDP groups were reduced to sulfhydryl groups by adding freshly prepared 150 mM dithiothreitol (DTT; Sigma–Aldrich) in PBS/EDTA-azide. $FNR_c$–PDP from both complexes or $FNR_r$–PDP were incubated with the thiol-terminated mica pieces to form covalent disulfide bonds between them.[20] The samples were extensively washed with PBS, 0.2% Tween 20 (Panreac) and 0.1% SDS (Panreac). For DFS measurements, saturated enzymatic layers were used as samples, whereas FNR samples with separated molecules were required to appreciate molecular recognition at the single-molecule level. The functionality of the tagged enzymes both immobilised and in solution was verified by using the cytochrome *c* reductase activity, as previously reported.[20]

### Tip Functionalisation

Maleimide-terminated flexible polyethylene glycol (PEG) linker silicon nitride AFM cantilevers (PEG, MW 3400; Novascan Technologies Inc., Ames, USA) were used. Cantilevers with nominal spring constants of 0.01–0.03 $N\,m^{-1}$ were calibrated by using the thermal noise method. $Fd_c$–PDP and $Fld_c$–PDP were reduced with 50 mM DTT for 30 min to expose the sulfhydryl groups. Cantilevers were incubated with 42 μM thiolated Fld/Fd in PBS/EDTA, pH 7.0, for 1 h, and washed extensively with the same buffer.

### Dynamic Force Spectroscopy (DFS)

AFM measurements were performed in a Cervantes FullMode SPM system (Nanotec Electrónica S.L, Spain). Several hundred Fz cycles were registered for Fd and Fld cantilever/FNR mica approaches at different $R$ values. Fz curves were obtained by applying a voltage to the z-piezo at a tip-retraction velocity from 80 to 4000 $nm\,s^{-1}$. These data translate into $R = 2$–80 $nN\,s^{-1}$. The curves were collected as voltage versus distance scans. The voltage values were transformed into force data by using the slope of the backward curve and the calibrated value of the spring constant of the functionalised cantilever. The measurements were performed for each type of FNR sample in PBS at room temperature. Negative control experiments were performed by blocking the available FNR sites by incubating the samples with a solution of 0.70 mM Fld in PBS. The loaded force between the tip and sample was kept constant and varied from 36 to 637 pN. Analysis of the efficiency of specific rupture events generated in the approaches was developed at different loading forces. From several thousand Fz curves collected by using the oriented $FNR_c$ samples, histograms of the specific unbinding forces were generated. Force histograms represent the frequency of peaks from Fz scans with rupture force values in small ranges with regard to all Fz scans with specific events. The histograms were created by using only peak force data from Fz curves that met the specificity requirements, that is, those Fz data with a force peak produced at a distance coinciding with the length of the spacer that binds the protein molecule to the tip and a shape that coincided with the corresponding PEG stretch.[41] The unbinding force histograms were fitted with multiple Gaussian functions by using the least-squares method. The first maxima found in fitting with lower values were assigned as one paired unbinding force, which was the most probable rupture force value; the other maxima were multiples of the first one.[42–45] Finally, the representation of the more probable unbinding forces versus $R$ was obtained by using the Evans–Ritchie expression,[8,46] which allowed us to estimate the dissociation rate constant at zero force, $k_{off}$, and the distance of the energy barrier with respect the ordinate axis, $x_\beta$, to characterise the mechanostability of the complexes.

### AFM Recognition Imaging

AFM recognition images were recorded by using force-based JM, which was able to map simultaneously the topography and adhesion properties of the surface sample.[47] By using the JM operation, forces applied to the sample could be precisely controlled to prevent soft samples from being damaged.[48] When JM operated by applying low forces in the repulsive regime with functionalised probes, the adhesion images might become quantitative recognition images.[22,23] The recognition images were developed by using Fd and Fld probes with an elasticity constant of 0.02 $N\,m^{-1}$ by applying a low force at $R = 10$ $nN\,s^{-1}$.

## Acknowledgements

*This work was supported by the Spanish MINECO (grant numbers BIO2013-42978-P and MAT2012-38318), the regional Gobierno de Aragón and MICINN-FEDER (grant B18 Biología Estructural). A.L. thanks ARAID for financial support. R.d.M. and C.M. are indebted to MICINN and DGA for receiving predoctoral fellowships. We also thank J. L. Díez and I. Echániz for technical support.*

**Keywords:** electron transfer · molecular recognition · redox chemistry · proteins · scanning probe microscopy

[1] D. D. Boehr, R. Nussinov, P. E. Wright, *Nat. Chem. Biol.* **2009**, *5*, 789–796.
[2] E. L. Florin, V. T. Moy, H. E. Gaub, *Science* **1994**, *264*, 415–417.
[3] G. U. Lee, L. A. Chrisey, R. J. Colton, *Science* **1994**, *266*, 771–773.
[4] E. Evans, A. Leung, D. Hammer, S. Simon, *Proc. Natl. Acad. Sci. USA* **2001**, *98*, 3784–3789.
[5] S. C. Kuo, M. P. Sheetz, *Science* **1993**, *260*, 232–234.
[6] C. A. Helm, W. Knoll, J. N. Israelachvili, *Proc. Natl. Acad. Sci. USA* **1991**, *88*, 8169–8173.
[7] N. Wang, J. P. Butler, D. E. Ingber, *Science* **1993**, *260*, 1124–1127.
[8] E. Evans, K. Ritchie, *Biophys. J.* **1997**, *72*, 1541–1555.
[9] D. J. Müller, Y. F. Dufrene, *Nat. Nanotechnol.* **2008**, *3*, 261–269.
[10] P. Hinterdorfer, Y. F. Dufrene, *Nat. Methods* **2006**, *3*, 347–355.
[11] M. Medina, C. Gomez-Moreno, *Photosynth. Res.* **2004**, *79*, 113–131.
[12] M. F. Fillat, W. E. Borrias, P. J. Weisbeek, *Biochem. J.* **1991**, *280*, 187–191.
[13] M. Martinez-Julvez, M. Medina, C. Gomez-Moreno, *J. Biol. Inorg. Chem.* **1999**, *4*, 568–578.
[14] M. Medina, R. Abagyan, C. Gomez-Moreno, J. Fernandez-Recio, *Proteins Struct. Funct. Bioinf.* **2008**, *72*, 848–862.
[15] M. Martinez-Julvez, M. Medina, A. Velazquez-Campoy, *Biophys. J.* **2009**, *96*, 4966–4975.
[16] V. Joosten, W. J. H. van Berkel, *Curr. Opin. Chem. Biol.* **2007**, *11*, 195–202.
[17] I. Willner, E. Katz, *Angew. Chem. Int. Ed.* **2000**, *39*, 1180–1218; *Angew. Chem.* **2000**, *112*, 1230–1269.
[18] G. Gilardi, A. Fantuzzi, *Trends Biotechnol.* **2001**, *19*, 468–476.
[19] P. B. Crowley, M. Ubbink, *Acc. Chem. Res.* **2003**, *36*, 723–730.
[20] C. Marcuello, R. de Miguel, C. Gomez-Moreno, M. Martinez-Julvez, A. Lostao, *Protein Eng. Des. Sel.* **2012**, *25*, 715–723.
[21] C. Marcuello, R. de Miguel, M. Medina, M. Martinez-Julvez, C. Gomez-Moreno, A. Lostao, *Febs J.* **2012**, *279*, 513–513.
[22] J. Sotres, A. Lostao, L. Wildling, A. Ebner, C. Gomez-Moreno, H. J. Gruber, P. Hinterdorfer, A. M. Baro, *ChemPhysChem* **2008**, *9*, 590–599.
[23] C. Marcuello, R. de Miguel, C. Gomez-Moreno, A. Lostao, *Eur. Biophys. J.* **2013**, *42*, S201–S201.
[24] H. A. Kramers, *Physica* **1940**, *7*, 284–304.
[25] F. Rico, V. T. Moy, *J. Mol. Recognit.* **2007**, *20*, 495–501.
[26] C. B. Yuan, A. Chen, P. Kolb, V. T. Moy, *Biochemistry* **2000**, *39*, 10219–10223.
[27] J. Foote, C. Milstein, *Nature* **1991**, *352*, 530–532.
[28] K. Matsui, J. J. Boniface, P. Steffner, P. A. Reay, M. M. Davis, *Proc. Natl. Acad. Sci. USA* **1994**, *91*, 12862–12866.
[29] P. Robert, A.-M. Benoliel, A. Pierres, P. Bongrand, *J. Mol. Recognit.* **2007**, *20*, 432–447.
[30] M. Medina, *Febs J.* **2009**, *276*, 3942–3958.
[31] G. Goñi, B. Herguedas, M. Hervas, J. R. Peregrina, M. A. De La Rosa, C. Gomez-Moreno, J. A. Navarro, J. A. Hermoso, M. Martinez-Julvez, M. Medina, *Biochim. Biophys. Acta Bioenerg.* **2009**, *1787*, 144–154.
[32] R. Merkel, P. Nassoy, A. Leung, K. Ritchie, E. Evans, *Nature* **1999**, *397*, 50–53.
[33] T. Mayoral, M. Martinez-Julvez, I. Perez-Dorado, J. Sanz-Aparicio, C. Gomez-Moreno, M. Medina, J. A. Hermoso, *Proteins Struct. Funct. Bioinf.* **2005**, *59*, 592–602.
[34] A. R. Bizzarri, S. Cannistraro, *Chem. Soc. Rev.* **2010**, *39*, 734–749.
[35] S. Allen, X. Y. Chen, J. Davies, M. C. Davies, A. C. Dawkes, J. C. Edwards, C. J. Roberts, J. Sefton, S. J. B. Tendler, P. M. Williams, *Biochemistry* **1997**, *36*, 7457–7463.

[36] A. Berquand, N. Xia, D. G. Castner, B. H. Clare, N. L. Abbott, V. Dupres, Y. Adriaensen, Y. F. Dufrene, *Langmuir* **2005**, *21*, 5517 – 5523.
[37] X. H. Zhang, S. E. Craig, H. Kirby, M. J. Humphries, V. T. Moy, *Biophys. J.* **2004**, *87*, 3470 – 3478.
[38] W. Baumgartner, P. Hinterdorfer, W. Ness, A. Raab, D. Vestweber, H. Schindler, D. Drenckhahn, *Proc. Natl. Acad. Sci. USA* **2000**, *97*, 4005 – 4010.
[39] B. Bonanni, A. S. M. Kamruzzahan, A. R. Bizzarri, C. Rankl, H. J. Gruber, P. Hinterdorfer, S. Cannistraro, *Biophys. J.* **2005**, *89*, 2783 – 2791.
[40] A. Díaz-Quintana„ J. A. Navarro, M. Hervás, F. P. Molina-Heredia, B. De La Cerda, M. A. De La Rosa, *Photosynth. Res.* **2003**, *75*, 97 – 110.
[41] C. Bouchiat, M. D. Wang, J. F. Allemand, T. Strick, S. M. Block, V. Croquette, *Biophys. J.* **1999**, *76*, 409 – 413.
[42] A. V. Krasnoslobodtsev, L. S. Shlyakhtenko, Y. L. Lyubchenko, *J. Mol. Biol.* **2007**, *365*, 1407 – 1416.
[43] C. Yan, A. Yersin, R. Afrin, H. Sekiguchi, A. Ikai, *Biophys. Chem.* **2009**, *144*, 72 – 77.
[44] E. J. Hukkanen, J. A. Wieland, A. Gewirth, D. E. Leckband, R. D. Braatz, *Biophys. J.* **2005**, *89*, 3434 – 3445.
[45] T. A. Sulchek, R. W. Friddle, K. Langry, E. Y. Lau, H. Albrecht, T. V. Ratto, S. J. DeNardo, M. E. Colvin, A. Noy, *Proc. Natl. Acad. Sci. USA* **2005**, *102*, 16638 – 16643.
[46] G. I. Bell, *Science* **1978**, *200*, 618 – 627.
[47] P. J. de Pablo, J. Colchero, J. Gomez-Herrero, A. M. Baro, *Appl. Phys. Lett.* **1998**, *73*, 3300 – 3302.
[48] J. Sotres, A. Lostao, C. Gomez-Moreno, A. M. Baro, *Ultramicroscopy* **2007**, *107*, 1207 – 1212.

Manuscript received: July 6, 2015
Accepted Article published: August 6, 2015
Final Article published: September 8, 2015